Structure of the 1,4-Bis(2′-deoxyadenosin-N^6-yl)-2*R*,3*R*-butanediol Cross-Link Arising from Alkylation of the Human *N-ras* Codon 61 by Butadiene Diepoxide†

W. Keither Merritt, Lubomir V. Nechev,‡ Tandace A. Scholdberg,§ Stephen M. Dean, Sarah E. Kiehna, Johanna C. Chang, Thomas M. Harris, Constance M. Harris, R. Stephen Lloyd,|| and Michael P. Stone*

Department of Chemistry, Center in Molecular Toxicology, Vanderbilt-Ingram Cancer Center, Vanderbilt University, Nashville, Tennessee 37235, and Center for Occupational and Environmental Toxicology, Oregon Health and Science University, 3181 SW Sam Jackson Park Road, L606, Portland, Oregon 97239-3098

Received December 31, 2004; Revised Manuscript Received May 4, 2005

ABSTRACT: The solution structure of the 1,4-bis(2′-deoxyadenosin-N^6-yl)-2*R*,3*R*-butanediol cross-link arising from N^6-dA alkylation of nearest-neighbor adenines by butadiene diepoxide (BDO_2) was determined in the oligodeoxynucleotide 5′-d(CGGACXYGAAG)-3′•5′-d(CTTCTTGTCCG)-3′. This oligodeoxynucleotide contained codon 61 (underlined) of the human *N-ras* protooncogene. The cross-link was accommodated in the major groove of duplex DNA. At the 5′-side of the cross-link there was a break in Watson−Crick base pairing at base pair X^6•T^{17}, whereas at the 3′-side of the cross-link at base pair Y^7•T^{16}, base pairing was intact. Molecular dynamics calculations carried out using a simulated annealing protocol, and restrained by a combination of 338 interproton distance restraints obtained from ^{1}H NOESY data and 151 torsion angle restraints obtained from ^{1}H and ^{31}P COSY data, yielded ensembles of structures with good convergence. Helicoidal analysis indicated an increase in base pair opening at base pair X^6•T^{17}, accompanied by a shift in the phosphodiester backbone torsion angle β P5′−O5′−C5′−C4′ at nucleotide X^6. The rMD calculations predicted that the DNA helix was not significantly bent by the presence of the four-carbon cross-link. This was corroborated by gel mobility assays of multimers containing nonhydroxylated four-carbon N^6,N^6-dA cross-links, which did not predict DNA bending. The rMD calculations suggested the presence of hydrogen bonding between the hydroxyl group located on the β-carbon of the four-carbon cross-link and T^{17} O^4, which perhaps stabilized the base pair opening at X^6•T^{17} and protected the T^{17} imino proton from solvent exchange. The opening of base pair X^6•T^{17} altered base stacking patterns at the cross-link site and induced slight unwinding of the DNA duplex. The structural data are interpreted in terms of biochemical data suggesting that this cross-link is bypassed by a variety of DNA polymerases, yet is significantly mutagenic [Kanuri, M., Nechev, L. V., Tamura, P. J., Harris, C. M., Harris, T. M., and Lloyd, R. S. (2002) *Chem. Res. Toxicol. 15*, 1572−1580].

1,3-Butadiene (CAS RN 106-99-0) (BD)[1] is used in the manufacture of styrene−butadiene rubber (SBR) (*1*, *2*); several billion pounds per year are produced in the United States. It is a combustion product from automobile emissions (*3*) and cigarette smoke (*4*). BD is genotoxic and is a carcinogen in rodents, particularly in mice (*5*−*7*) and also in rats (*8*). BD was classified by the United States Environmental Protection Agency as "carcinogenic to humans by inhalation" (*9*). The International Agency for Cancer Research (IARC) lists BD as a "probable human carcinogen" (group 2A) (*10*−*12*). Chronic human exposure in the SBR industry may induce genotoxic effects (*13*−*15*) and is correlated with increased risk for leukemia (*1*, *16*−*24*).

BD is epoxidized primarily by cytochrome P450 2E1, but also by cytochrome P450 2A6, to form 1,2-epoxy-3-butenes (BDO) (Scheme 1) (*25*, *26*). These may be further oxidized by cytochrome P450 2E1 or 3A4 to form 1,2:3,4-diepoxybutanes (BDO_2) (*25*, *27*−*31*). Hydrolysis of BDO mediated by epoxide hydrolase forms 1,2-dihydroxy-3-butenes (*29*, *32*, *33*), which are metabolized by cytochrome P450 to hydroxymethyl vinyl ketone (HMVK) (*34*). Either BDO_2 or the 1,2-dihydroxy-3-butenes undergo cytochrome P450-mediated oxidation to form 1,2-dihydroxy-3,4-epoxybutanes (BDE) (*29*, *32*, *35*). Thus, proximate electrophiles arising from BD metabolism include BDO, BDO_2, and BDE, and, potentially, HMVK (*36*).

† This work was supported by NIH Grants ES-05509 (M.P.S.) and ES-05355 (T.M.H. and R.S.L.). Funding for the NMR spectrometers was supplied by Vanderbilt University, by NIH Grant RR-05805, and by the Vanderbilt Center in Molecular Toxicology, ES-00267. The Vanderbilt-Ingram Cancer Center is supported by NIH Grant CA-68485.

* To whom correspondence should be addressed. Telephone: 615-322-2589. Fax: 615-322-7591. E-mail: michael.p.stone@vanderbilt.edu.

‡ Current address: Alnylam Pharmaceuticals, 790 Memorial Drive, Suite 202, Cambridge, MA 02139.

|| Oregon Health and Science University.

§ Current address: U.S.D.A., 10383 North Ambassador Dr., Kansas City, MO 64153.

[1] Abbreviations: BD, butadiene; BDE, 3,4-epoxy-1,2-butanediol; BDO, butadiene monoepoxide (1,2-epoxy-3-butene); BDO_2, butadiene diepoxide (1,2:3,4-diepoxybutane); BDT, butadienetriol; CPK, Corey−Pauling−Koltun space-filling models; DQF-COSY, double-quantum-filtered correlation spectroscopy; HMBC, heteronuclear multiple bond correlation spectroscopy; HMVK, hydroxymethyl vinyl ketone; MALDI-TOF, matrix-assisted laser desorption ionization time-of-flight mass spectrometry; NOE, nuclear Overhauser enhancement; NOESY, nuclear Overhauser enhancement spectroscopy; R_1^x, sixth root residual; rMD, restrained molecular dynamics; rmsd, root mean square deviation; SBR, styrene−butadiene rubber; TBE, Tris−borate−EDTA buffer; TOCSY, total correlation spectroscopy; TPPI, time-proportional phase increment.

10.1021/bi047263g CCC: $30.25
Published on Web 07/08/2005

Scheme 1: Reactive Metabolites of Butadiene

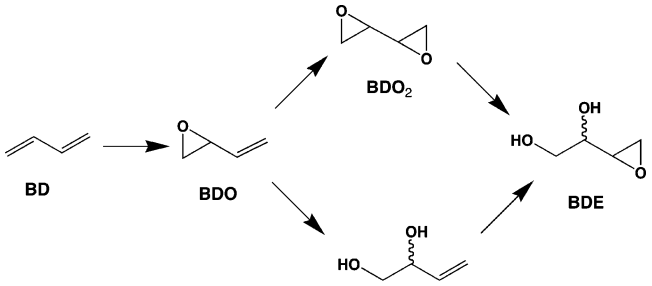

Scheme 2: The *ras61* Oligodeoxynucleotide (A) and the Chemical Structure of (B) the (2*R*,3*R*)-N^6-(2,3-Dihydroxybutyl)-2-deoxyadenosyl Cross-Link Adduct and Nomenclature

A.

60 61 62

5′-C^1 |G^2 G^3 A^4 |C^5 X^6 Y^7 |G^8 A^9 A^{10}|G^{11}-3′

3′-G^{22}|$C^{21}C^{20}T^{19}$|$G^{18}T^{17}T^{16}$|$C^{15}T^{14}T^{13}$|C^{12}-5′

B.

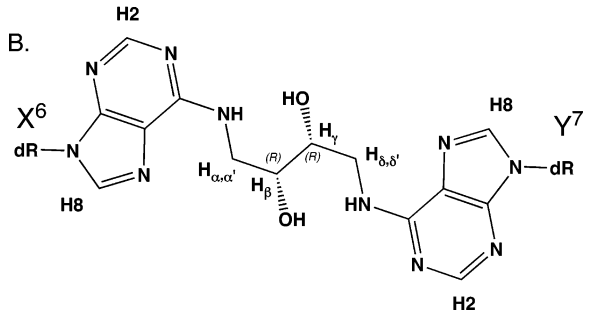

The diepoxide BDO_2 is highly genotoxic (*2*, *10*, *37*), probably due to its potential to form DNA−DNA (*38*−*41*) and DNA−protein cross-links, the latter of which have been observed in mice (*42*, *43*). Mice have been shown to possess greater sensitivity to butadiene exposure than rats, and this is attributed to their efficient oxidation of BD to BDO_2 (*44*, *45*), presumably facilitating DNA cross-linking. Butadiene genotoxicty was further enhanced in knockout mice lacking a functional microsomal epoxide hydrolase gene (*46*). Polymorphisms in the human epoxide hydrolase gene may also contribute to differences in BD genotoxicty within the human population (*47*, *48*).

The predominant DNA cross-link induced by BDO_2 involves interstrand bisalkylation at N7-dG in 5′-GNC-3′ sequences (*40*). This cross-link was isolated from DNA and characterized by mass spectrometry (*41*). Recently, additional guanine−adenine DNA interstrand cross-links induced by BDO_2, including an N7-dG−N^6-dA cross-link, were characterized by mass spectrometry (*49*). The recovery of an interstrand cross-link involving N^6-dA was significant since, with respect to alkylation by butadiene epoxide, the N^6-dA exocyclic amine is less reactive than the N1 imine. The prevailing hypothesis posits that N^6-alkylation products of butadiene epoxides result from initial alkylation at the N1 position, followed by Dimroth rearrangement (*50*, *51*). The BDT N1-dA adduct has been identified in humans exposed occupationally to BD (*52*). The N^6-dA BDT adduct was identified in Chinese hamster ovary cells (*53*).

The bisalkylation of tandem deoxyadenosines to yield intrastrand (*R*,*R*)-N^6,N^6-dA cross-links is anticipated to be a rare occurrence. This adduct has not yet been reported from mass spectrometry analysis of DNA exposed to BDO_2 (*49*, *54*). However, its synthetic accessibility (*55*) facilitated biochemical structure−activity studies. As compared to N^6-dA monoadducts arising from BDO or BDE (*56*, *57*), the (*R*,*R*)-N^6,N^6-dA cross-link was significantly more mutagenic. It was examined as to site-specific mutagenesis, both in *Escherichia coli* and in COS-7 cells (*55*). In both systems, the primary mutations were A → G transitions observed at the 3′-adenine of the cross-link. The levels of mutations observed in the COS-7 cells were significantly greater than were observed in the bacterial system.

Both the *R*,*R* and *S*,*S* stereoisomers of this N^6,N^6-dA intrastrand cross-link were bypassed by a variety of DNA polymerases in vitro (*55*), suggesting that they did not pose severe blocks to replication; mutagenesis in *E. coli* may be due to DNA polymerase II-mediated lesion bypass (*58*). It was proposed that these BDO_2-induced cross-links were accommodated within the major groove, similar to several N^6-dA adducts of styrene oxide, which also did not pose severe blocks to replication (*59*, *60*). This was in contrast to the corresponding (*R*,*R*)- and (*S*,*S*)-N^2,N^2-dG intrastrand cross-links, which were severe replication blocks when examined in vitro (*61*).

The present work characterizes structural perturbation to the *ras61* oligodeoxynucleotide caused by the 1,4-bis(2′-deoxyadenosin-N^6-yl)-2*R*,3*R*-butanediol cross-link. Molecular dynamics calculations restrained by interproton distances and torsion angle restraints obtained from NMR spectroscopy indicate that the cross-linked moiety is accommodated in the major groove of the DNA double helix. Watson−Crick base pairing is disrupted at position X^6•T^{17}, the 5′-side of the intrastrand cross-link. Helicoidal analysis suggests an opening of this base pair. Potential hydrogen bond formation between the β-hydroxyl group of the cross-link and T^{17} O^4, the nucleotide complementary to X^6, shields the T^{17} imino hydrogen from exchange with solvent. In contrast, Watson−Crick base pairing is intact at position Y^7•T^{16}, the 3′-side of the cross-link.

MATERIALS AND METHODS

Sample Preparation. The oligodeoxynucleotides 5′-d(CGGACAAGAAG)-3′ and 5′-d(CTTCTTGTCCG)-3′ were synthesized by the Midland Certified Reagent Co. (Midland, TX) and purified by anion-exchange chromatography. The cross-linked oligodeoxynucleotide 5′-d(CGGAC<u>XY</u>GAAG)-3′ was synthesized by a variation of the postoligomerization method described for the preparation of monoadducts of butadiene epoxides (*55*, *62*). The concentrations of the single-stranded oligonucleotides were determined from their calculated extinction coefficients at 260 nm (*63*). The modified oligodeoxynucleotide and its complement were annealed in a buffer consisting of 10 mM NaH_2PO_4, 0.1 M NaCl, and 50 μM Na_2EDTA at pH 7.0. The modified duplex was eluted from DNA grade Bio-Gel hydroxylapatite (Bio-Rad Laboratories, Hercules, CA) with a gradient from 10 to 200 mM NaH_2PO_4, pH 7.0. It was desalted using Sephadex G-25.

Capillary Gel Electrophoresis. The purity of the modified duplex was analyzed using a PACE 5500 (Beckman Instru-

ments, Inc., Fullerton, CA) instrument. Electrophoresis was conducted using an eCAP ssDNA 100-R kit applying 12000 V for 30 min. The electropherogram was monitored at 254 nm.

Mass Spectrometry. MALDI-TOF mass spectra were measured on a Voyager-DE (PerSeptive Biosystems, Inc., Foster City, CA) instrument in negative reflector mode. The matrix contained 0.5 M 3-hydroxypicolinic acid and 0.1 M ammonium citrate.

Thermal Melting. Thermal melting of duplex DNA was monitored using UV spectroscopy at 260 nm in a buffer consisting of 1 M NaCl, 10 mM Na_2HPO_4, 10 mM NaH_2PO_4, and 50 μM Na_2EDTA at pH 7.0. Melting temperatures were determined by measuring the absorbance change as a function of temperature; the temperature range was 15−85 °C with a 1 °C/min increment.

Electrophoretic Mobility. Adducted or unmodified oligodeoxynucleotides were combined individually with excess complement 5′-d(CGCTTCTTGTC). They were phosphorylated with 3.8 units of T4 polynucleotide kinase and 20.8 μL of 10 μM ATP at 37 °C in 6 μL of 10× DNA kinase buffer (70 mM Tris-HCl, pH 7.6, 10 mM $MgCl_2$, 5 mM dithiothreitol) (pH 7.6) and incubated overnight at 37 °C with an additional 1.9 units of kinase and 10.4 μL of 10 μM ATP. *Bam*HI linker [5′-d$(CGGGATCCCG)_2$-3′] was phosphorylated with 1.9 units of T4 polynucleotide kinase in 2 μL of 10× kinase buffer and 10.4 μL of 10 μM ATP and incubated overnight at 37 °C. Fractions of each reaction (*Bam*HI, 0.025 A_{260} units; unmodified, 0.02 A_{260} units; four-carbon linker, 0.04 A_{260} units) were removed and incubated with T4 DNA ligase (*Bam*HI, 5 units; unmodified, 2 units; four-carbon linker, 2 units) in 2 μL of 10× T4 DNA ligase buffer (50 mM Tris-HCl, 10 mM $MgCl_2$, 10 mM dithiothreitol, 1 mM ATP, 5 μg/mL bovine serum albumin) (pH 7.8) and 10 μL of 10 μM ATP overnight at 16 °C and precipitated with absolute ethanol. They were suspended in 6 mL of nondenaturing loading buffer (Sigma). One microliter of a pBR322 *Hae*III digest (0.4 μg/mL, 10 mM Tris-HCl, 0.1 mM Na_2EDTA) (pH 8.0) was mixed with nondenaturing loading buffer per each length marker lane. Electrophoresis was performed using a nondenaturing 8% polyacrylamide gel (monoacrylamide:bisacrylamide ratio 29:1, 3.3% catalyst). Gels were run at 1000 V for 2.5−3 h and stained for 30 min with 250 mL of GelStar nucleic acid stain (10000×) (Biowhittaker Molecular Applications, Walkersville, ME) in 250 mL of 1× TBE. Gels were imaged on a UV transilluminator (Alpha Innotech, San Leandro, CA). Control multimers formed by ligation of the 10-bp *Bam*HI linker were used to calculate apparent lengths of cross-linked multimers.

NMR. The modified duplex was prepared at a concentration of 2 mM. For observation of nonexchangeable protons, the sample was dissolved in 0.5 mL of 99.96% D_2O containing 10 mM NaH_2PO_4, 0.1 M NaCl, and 50 μM Na_2EDTA (pH 7.0). For observation of exchangeable protons, the sample was dissolved in 0.5 mL of 9:1 H_2O:D_2O in the same buffer. ^{1}H NMR spectra were recorded at 600.13 and 800.23 MHz. The nonexchangeable protons were monitored at 25 °C; the exchangeable protons were monitored at 17 °C. Chemical shifts were referenced to water. Data were processed using the program FELIX2000 (Accelrys, Inc., San Diego, CA). NOESY spectra of nonexchangeable protons were recorded using TPPI phase cycling with mixing times of 150, 200, and 250 ms. Spectra for exchangeable protons were recorded using a 150 ms mixing time. These were recorded with 1024 real data points in the d_1 dimension and 2048 real data points in the d_2 dimension. A relaxation delay of 2.0 s was used. Water suppression was performed using the WATERGATE sequence (*64*). TOCSY experiments were performed with mixing times of 90 and 150 ms, utilizing homonuclear Hartman−Hahn transfer with the MLEV17 sequence (*65*) for mixing. DQF-COSY spectra were zero-filled to give a matrix of 1024 × 2048 real points. A skewed sine-bell square apodization function with a 90° phase shift and a skew factor of 1.0 was used in both dimensions.

Experimental Restraints. (a) Distance Restraints. Footprints were drawn around cross-peaks obtained at a mixing time of 200 ms using FELIX2000. Identical footprints were transferred and fit to the cross-peaks obtained at the other two mixing times. The intensities of cross-peaks were determined by volume integrations. These were combined as necessary with intensities generated from complete relaxation matrix analysis of a starting DNA structure to generate a hybrid intensity matrix (*66*, *67*). MARDIGRAS (*68*−*70*) was used to iteratively refine the hybrid intensity matrix and to optimize the agreement between the calculated and experimental NOE intensities. Calculations were initated using isotropic correlation times of 2, 3, and 4 ns and with both IniA and IniB starting structures and the three mixing times, yielding eighteen sets of distances. Analysis of these data yielded the experimental distance restraints used in subsequent restrained molecular dynamics calculations and the corresponding standard deviations for the distance restraints. The distance restraints were divided into five classes, reflecting the confidence level in the experimental data.

(b) Torsion Angle Restraints. Deoxyribose pseudorotation (*57*) was determined graphically using the sums of ^3J ^{1}H coupling constants (*58*), measured from DQF-COSY spectra. Discrete $J_{1'2''}$ and $J_{1'2'}$ couplings were measured from active and passive couplings, respectively, of the H2″ (d_2) to H1′ (d_1) spectral region. The data were fit to curves relating the coupling constants to the deoxyribose sugar pseudorotation angle (P), sugar pucker amplitude (ϕ), and the percentage S-type conformation. The sugar pseudorotation angle and amplitude ranges were converted to the five dihedral angles ν_0 to ν_4. Coupling constants measured from ^{1}H−^{31}P HMBC spectra were applied (*71*, *72*) to the Karplus relationship (*73*) to determine the backbone dihedral angle ϵ (C4′−C3′−O3′−P), related to the H3′−C3′−O3′−P angle by a 120° shift. The ζ (C3′−O3′−P−O5′) backbone angles were calculated from the correlation between ϵ and ζ in B-DNA (*60*).

Restrained Molecular Dynamics Calculations. Classical A-DNA and B-DNA were used as reference structures to create starting structures for the refinement (*74*). The butadiene adduct was constructed at A^6 and bonded to A^7 using the BUILDER module of INSIGHT II (Accelrys). A-form and B-form structures of the appropriate sequence were energy-minimized by the conjugate gradients method for 200 iterations using the AMBER 7.0 force field (*75*) without experimental restraints to give starting IniA and IniB used for the subsequent relaxation matrix analysis and molecular dynamics calculations. The restraint energy function included terms describing distances and dihedral restraints as square-well potentials (*76*). Bond lengths involving

hydrogens were fixed with the SHAKE algorithm (*77*). The generalized Born approach was used to model solvent (*78*, *79*). The calculations utilized a salt concentration of 0.2 mM. A series of randomly seeded rMD calculations were performed over a time course of 40 ps. These used the SANDER module of AMBER 7.0 and the Cornell et al. force field (*80*), including the Parm94.dat parameter set. The simulated annealing protocol utilized a starting temperature of 25 K. In the first picosecond the temperature was increased to 600 K. This was maintained for 4 ps, followed by cooling to 298 K over 15 ps. During the final 20 ps the temperature was reduced to 0 K. Temperature was controlled by coupling to a temperature bath. During the first 1 ps of heating a coupling of 0.4 ps was used. During the next 4 ps of constant temperature dynamics a coupling of 1.0 ps was used. In the first 15 ps of cooling, a value of 1.0 ps was used, followed by a value of 0.5 ps for the second 15 ps. During the final 5 ps of cooling, the coupling was ramped down to 0.01 ps. In the first 1 ps of heating, the experimental force constants were amplified by factors that ranged from 0.5 to 1.00. During the 4 ps of constant temperature dynamics and the first 15 ps of cooling, the amplification factor was increased to 1.75. In the final 20 ps of cooling, the amplification factor was reduced to 1.0. Structure coordinates were archived every 0.1 ps over the final 10 ps of the simulation. Structure coordinates extracted from the final 4 ps were averaged and energy-minimized for 200 iterations using the conjugate gradients algorithm. An average structure was obtained from eight randomly seeded rMD calculations. Back-calculation of ^{1}H NOE data was performed using CORMA (version 4.0) (*66*, *67*). Helicoidal parameters were examined using 3DNA (*81*).

Table 1: Analysis of the rMD-Generated Structures of the *ras61* (*R*,*R*)-N^6,N^6-dA Cross-Linked Adduct

NMR restraints	
total no. of distance restraints	338
interresidue distance restraints	91
intraresidue distance restraints	247
DNA cross-link distance restraints	0
torsion angle restraints	
sugar pucker restraints	80
backbone torsion angle restraints	71
empirical restraints	
H-bonding restraints	46
dihedral planarity restraints (in X-PLOR)	20
structural statistics	
NMR *R*-factor (R_1^x)[a]	1.12×10^{-1}
rmsd of NOE violations (Å)	2.15×10^{-2}
no. of NOE violations >0.15 Å	9
pairwise rmsd (Å) over all atoms	
IniA vs IniB	5.92
IniA vs $rMDA_{av}$	4.75
IniB vs $rMDB_{av}$	2.50
rMDA vs rMDB	0.90
rMDA vs rMDA	0.51
rMDB vs rMDB	0.81
⟨rMDA⟩ vs $rMDA_{av}$	0.33 ± 0.11
⟨rMDB⟩ vs $rMDB_{av}$	0.52 ± 0.21

[a] The mixing time was 150 ms. $R_1^x = \sum|(a_o)_i^{1/6} - (a_c)_i^{1/6}|/\sum|(a_o)_i^{1/6}|$, where a_o and a_c are the intensities of observed (nonzero) and calculated NOE cross-peaks. ⟨rMDA⟩ represents a group of six converged structures starting from IniA; ⟨rMDB⟩ represents a group of six converged structures starting from IniB. $rMDA_{av}$ represents the potential energy minimized average structure of all six rMD calculations starting with A-form DNA. $rMDB_{av}$ represents the potential energy minimized average structure of all eight rMD calculations starting with B-form DNA. The comparisons, rMDA vs rMDB, rMDA vs rMDA, and rMDB vs rMDB, represent the maximum observed pairwise rmsd over all atoms between these groups.

RESULTS

Sample Properties. The purity of the (*R*,*R*)-N^6,N^6-dA cross-linked adduct duplex was assessed using capillary gel electrophoresis. The electropherogram exhibited two peaks in a 1:1 ratio after correction for the respective absorbance coefficients. The identity of the duplex was verified using MALDI-TOF mass spectrometry. Mass measurement showed two signals that corresponded to mass units of 3484 and 3272. These peaks corresponded to the cross-linked adduct strand 5′-d(CGGAC<u>XY</u>GAAG)-3′ and to the complementary strand 5′-d(CTTCTTGTCCG)-3′, respectively. The melting temperature of the sample was determined by UV spectroscopy as 50 °C, less than the observed 57 °C melting temperature of the unmodified *ras61* duplex. The cross-link sample yielded excellent NMR data in the temperature range of 10−25 °C.

DNA ^{1}H Resonance Assignments. (a) Nonexchangeable Protons. The sequential NOEs between the aromatic and anomeric protons are displayed in Figure 1. These were assigned using standard methods (*82*, *83*). There were no breaks observed in connectivity in either the cross-linked strand or the complementary strand. With assignments of the sugar H1′ protons in hand, the remainder of the deoxyribose sugar protons were assigned from DQF-COSY spectra. With the exception of several of the H5′ and H5″ protons, assignments of the sugar protons were made unequivocally. Table S1 in the Supporting Information details the complete nonexchangeable ^{1}H NMR assignments of the cross-linked adduct oligodeoxynucleotide duplex.

(b) Exchangeable Protons. An expanded region showing the far downfield region of the ^{1}H NMR spectrum, exhibiting cross-peaks between the hydrogen-bonded imino protons, is shown in Figure 2. Sequential assignments of the imino protons from base pairs G^2•$C^{21} \rightarrow C^5$•G^{18} and X^6•$T^{17} \rightarrow A^{10}$•$T^{13}$ were obtained, with a break in connectivity observed between base pairs C^5•G^{18} and X^6•T^{17}. The NOE between T^{13} N3H and T^{14} N3H was weak. It was not observed at the contour level plotted in Figure 2. This cross-peak was also weak in the *ras61* spectrum (*84*) and presumably reflected the effects of strand fraying and resulting rapid exchange of this proton with solvent. Each of the peaks identified in the cytosine amino region of the ^{1}H NMR spectrum exhibited the anticipated cross-peak with the appropriate deoxyguanosine imino proton as expected in Watson−Crick base pairing. With the exception of T^{16}, each thymine N3H proton exhibited an NOE to the corresponding adenine H2 proton in the complementary strand. Cross-peaks were observed between T^{17} N3H and the T^{16} CH_3 and T^{17} CH_3 resonances.

(c) Butadiene Protons. The protons of the butadiene cross-link were observed as separate resonances, with spectral line widths comparable to the oligodeoxynucleotide protons (Figure 3).[2] At a mixing time of 200 ms, NOEs were observed between the butadiene cross-link protons. The $H_{\alpha''}$

[2] The definitions of the prochiral protons at C_α and C_δ of the N^6,N^6-dA cross-link moiety are based upon the Cahn, Ingold, and Prelog nomenclature. The proton H_α is defined as the *pro-R* proton at C_α; $H_{\alpha'}$ is defined as the *pro-S* proton at C_α. Likewise, H_δ is the *pro-R* proton at C_δ; $H_{\delta'}$ is the *pro-S* proton at C_δ.

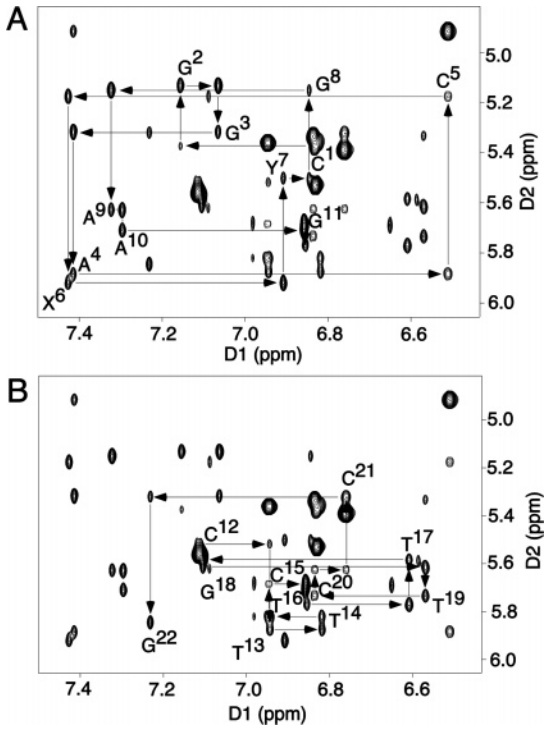

FIGURE 1: Expanded plots of a NOESY spectrum at a mixing time of 200 ms showing sequential NOE connnectivities from aromatic to anomeric protons of the (*R*,*R*)-BD-(61,2−3) cross-linked adduct. (A) Nucleotides $C^1 \rightarrow G^{11}$ of the modified strand. (B) Nucleotides $C^{12} \rightarrow G^{22}$ of the complementary strand.

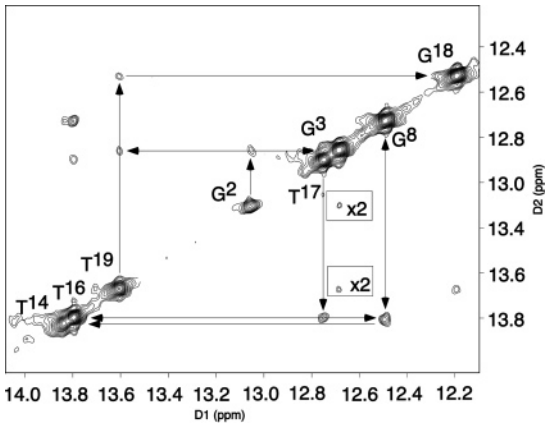

FIGURE 2: Expanded plot of a NOESY spectrum at a mixing time of 200 ms showing NOE connectivities for the imino protons for the base pairs from $G^2 \cdot C^{21}$ to $A^{10} \cdot T^{13}$. Note that there is a break in the walk between the imino resonances for base pairs $G^2 \cdot C^{21}$ and $X^6 \cdot T^{17}$. The resonance observed for base pair $X^6 \cdot T^{17}$ is shifted in the spectrum.

proton at 3.51 ppm showed NOEs to H_β at 4.03 ppm and $H_{\alpha'}$ at 2.72 ppm. The H_β proton showed NOEs to $H_{\alpha'}$ and $H_{\alpha''}$, along with a weak NOE to H_γ at 3.62 ppm and $H_{\delta''}$ at 3.26 ppm. The H_γ proton showed a weak NOE to H_β (not observed in Figure 3) along with NOEs to $H_{\delta'}$ at 3.01 ppm and $H_{\delta''}$, respectively. A cross-peak was observed between T^{17} N3H and the $H_{\delta'}$ proton of the cross-link (Figure 4). This was the only cross-peak observed between the butadiene cross-link and the oligodeoxynucleotide.

Torsion Angle Measurements. Analysis of DQF-COSY data suggested that all deoxyribose pseudorotation angles remained in the C2′-endo range anticipated for B-family DNA. The glycosyl torsion angles were monitored using ^1H

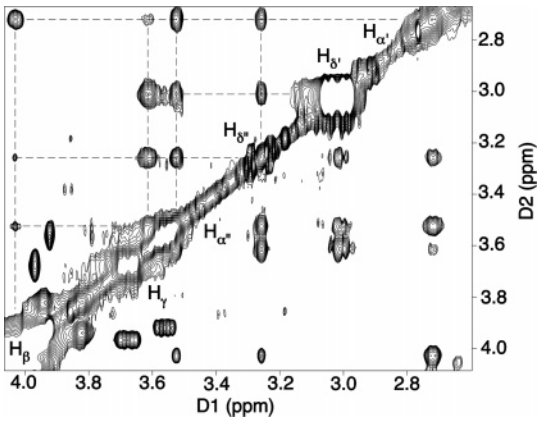

FIGURE 3: Expanded NOESY spectrum at 200 ms mixing time exhibiting the assignment of cross-link protons in the (*R*,*R*)-BD-(61,2−3) cross-linked adduct duplex. The experiment was at 800.23 MHz and 25 °C.

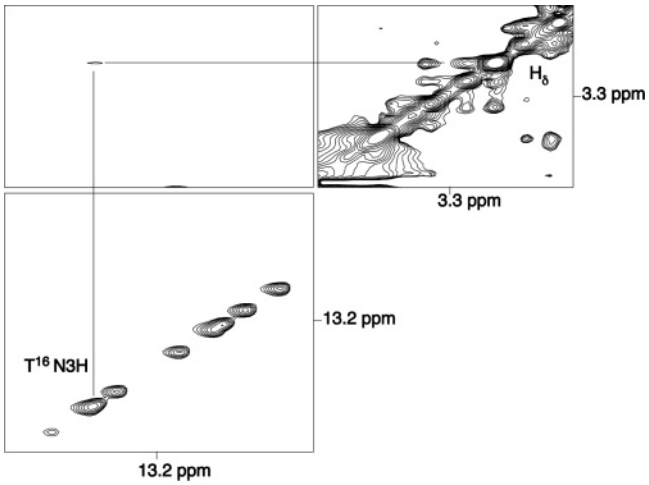

FIGURE 4: NOE observed between T^{16} N3H and the $H_{\delta'}$ proton of the (*R*,*R*)-BD-(61,2−3) cross-linked adduct. The experiment was at 800.23 MHz and 17 °C.

NOESY experiments. These revealed weak NOEs between the purine H8 or pyrimidine H6 protons and the anomeric H1′ protons of the attached deoxyribose sugars, consistent with glycosyl torsion angles in the normal *anti* conformational range. There were also no unusual chemical shifts or $^3J_{^1H-^{31}P}$ couplings observed in the ^{31}P spectrum. Data obtained from $^3J_{^1H-^{31}P}$ experiments indicated that the torsion angles associated with the backbone phosphodiester linkages were not significantly perturbed by the presence of the cross-link. Karplus analysis yielded values within the standard ranges of 165.0° ± 10° and 235° ± 10° for the backbone torsion angles ϵ and ζ, respectively (*85*).

Chemical Shift Effects. The ^1H chemical shifts of the cross-linked duplex were compared to those of the unmodified *ras61* oligomer (*84*). Figure 5 shows that chemical shift differences were localized in the cross-linked strand at the two cross-linked nucleotides X^6 and Y^7. The X^6 H1′ resonance shifted 0.6 ppm upfield, while the Y^7 H8 resonance shifted 0.4 ppm downfield. In the far downfield region of the ^1H spectrum, the T^{17} N3H imino resonance shifted upfield approximately 1.0 ppm. The complementary strand did not exhibit significant changes in ^1H chemical shifts.

Structural Refinement. The structural refinement incorporated 338 experimental distance restraints. There was one

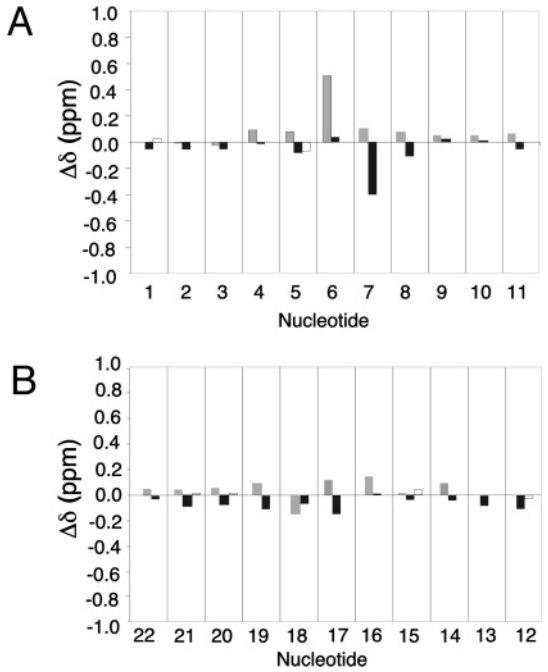

FIGURE 5: Chemical shift differences of protons of the (*R*,*R*)-BD-(61,2−3) cross-linked adduct duplex relative to the unmodified *ras61* oligodeoxynucleotide. (A) The modified strand of the cross-linked adduct. (B) The complementary strand of the cross-linked adduct. Gray bars represent the deoxyribose H1′ protons; black bars represent the purine H8 or pyrimidine H6 protons, respectively.

NOE observed between the cross-linked butadiene moiety and the DNA. The distance restraints were evenly distributed over the length of the cross-linked oligodeoxynucleotide. In addition, 80 deoxyribose pseudorotation restraints were included. There were 106 phosphodiester backbone torsion angle restraints. The phosphodiester backbone angles ϵ and ζ were restrained at angles of 165° ± 10° and 245° ± 10°, respectively. Empirical Watson−Crick hydrogen-bonding restraints were used for all base pairs except for X^6•T^{17}, as NMR data indicated no base pairing at this site. Inspection of the structures that emerged from an initial series of randomly seeded rMD calculations suggested that the C_β hydroxyl of the cross-link and T^{17} O^4 were within hydrogen-bonding distance. It was therefore decided to add an empirical restraint for this hydrogen bond in subsequent calculations.

A stereoview of six energy-minimized structures emergent from the rMD calculations is shown in Figure 6. These rMD calculations were initiated from both the A-form and B-form starting structures. These two starting structures exhibited an rmsd of 5.92 Å. The rMD calculations converged to similar ensembles of structures irrespective of starting structure. The maximum pairwise rmsd between these emergent structures was 0.90 Å, suggesting that the experimental distance and torsion angle restraints, combined with the additional empirical hydrogen-bonding restraints, enabled the rMD calculations to converge to a well-defined set of structures. The average structure emergent from the rMD calculations exhibited a rmsd of 2.50 Å as compared to the IniB starting structure. This deviation from canonical B-form DNA resulted primarily from structural variation associated with the cross-linked base pairs X^6•T^{17} and Y^7•T^{16}.

The validities of the structures emergent from the rMD calculations were evaluated using complete relaxation matrix

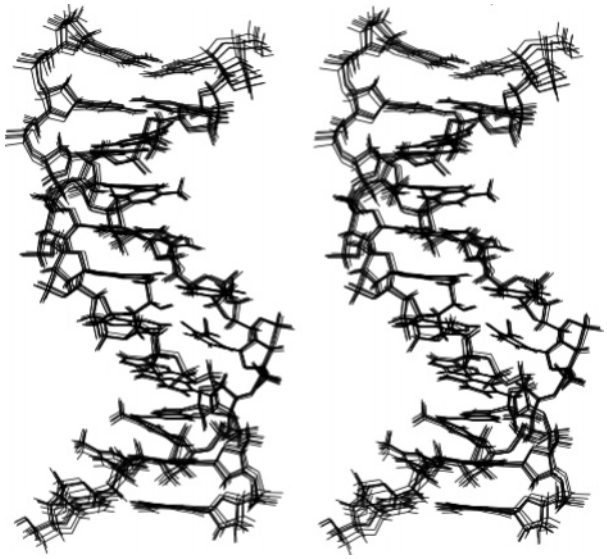

FIGURE 6: A stereoview of six superimposed structures emergent from the simulated annealing rMD protocol; the structures resulted from randomly seeded calculations.

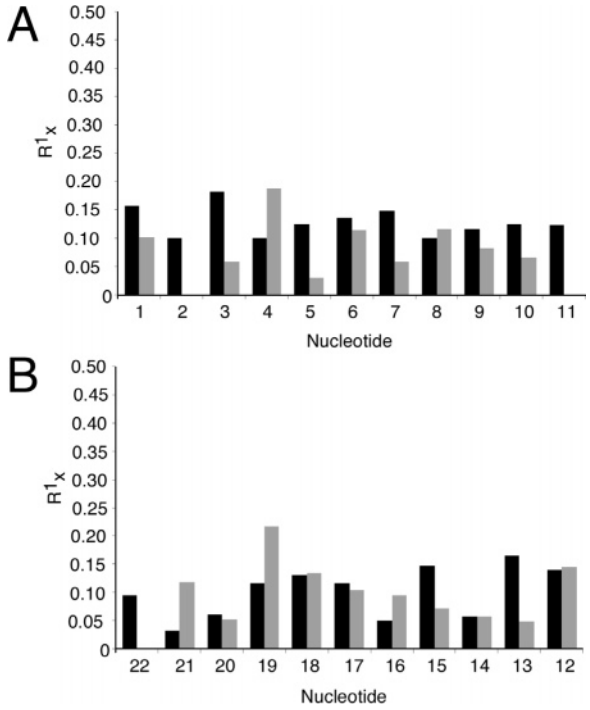

FIGURE 7: R_1^x values as a function of position in the (*R*,*R*)-BD-(61,2−3) cross-linked adduct. (A) The cross-linked strand. (B) The complementary strand. The black bars represent intranucleotide R_1^x values, and the white bars represent internucleotide R_1^x values.

calculations (*66*, *67*). Figure 7 shows R_1^x values as a function of nucleotide position. The residual values were consistent over the length of the modified oligodeoxynucleotide and ranged from 3.1 to 14.8 × 10^{-2}. The inclusion of the empirical hydrogen-bonding restraint between the C_β hydroxyl of the cross-linked adduct and T^{17} O^4 resulted in a 10% improvement in the R_1^x residual for base step C^5 → X^6, as compared to the corresponding calculations in which this empirical restraint was not utilized.

Structure of the (R,R)-BD-(61−2,3) Cross-Linked Adduct. The structures that emerged from the rMD calculations indicated that the N^6,N^6-dA butadiene cross-link oriented in the major groove of the DNA, as shown in Figure 8.

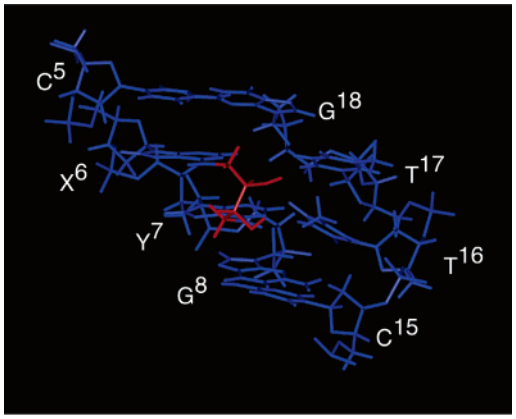

FIGURE 8: A close-up view of the (*R*,*R*)-BD-(61,2−3) cross-linked duplex. View from the major groove of X^6•T^{17} and Y^7•T^{16} and the flanking base pairs C^5•G^{18} and G^8•C^{15}. The duplex DNA is shown in blue; the cross-link is in red.

Watson−Crick base pairing was disrupted at X^6•T^{17}. In contrast, base pairing at Y^7•T^{16} was maintained. Helicoidal analysis (*81*) suggested a change of the phosphodiester backbone torsion angle β, P5′−O5′−C5′−C4′, at X^6. In the presence of the N^6,N^6-dA cross-link, angle β at X^6 increased to approximately 200°, as compared to the expected range of 165−180°. The emergent structures suggested the formation of a hydrogen bond between the C_β hydroxyl of the butadiene cross-link and T^{17} O^4, thus stabilizing nucleotide T^{17} in the complementary strand in the absence of Watson−Crick hydrogen bonding with cross-linked nucleotide X^6.

The structures that emerged from the rMD calculations suggested that the four-carbon N^6,N^6-dA cross-link did not bend the DNA duplex. To confirm this observation, a series of electrophoretic mobility assays were conducted on ligated multimers of an oligodeoxynucleotide containing the nonhydroxylated analogue of the N^6,N^6-dA cross-link. Thermal melting studies monitored by UV spectroscopy indicated that the nonhydroxylated alkyl tether also lowered the T_m of the duplex by approximately 6°, as observed for the hydroxylated N^6,N^6-dA cross-link, suggesting that the nonhydroxylated alkyl tether provided a reasonable model for the N^6,N^6-dA cross-linked oligodeoxynucleotide studied by NMR. The mobilities of the ligated cross-linked multimers were analyzed by nondenaturing polyacrylamide gel electrophoresis (*86*). The electrophoretic migration data corroborated NMR data suggesting that this cross-linked oligodeoxynucleotide did not undergo significant bending.

The base-stacking patterns at the cross-link site are shown in Figure 9. Helicoidal analysis suggested a decrease in the base pair opening parameter at base pair X^6•T^{17}, from the expected range of 0 ± 5° (base pair closed) to a value of approximately −13°. Intrastrand cross-link formation was accompanied by a decrease in the twist angle between base pairs C^5•G^{18} and X^6•T^{17}, resulting in unwinding of the duplex. Consequently, in the cross-linked structure, nucleotides X^6 and Y^7 did not exhibit the typical 36° twist as was observed for the monodentate butadienetriol adduct located at position X^6 or for the unmodified *ras61* oligodeoxynucleotide. The opening of the duplex at X^6•T^{17} resulted in the six-carbon pyrimidine ring of the X^6 purine stacking above the imidazole ring of the Y^7 purine. In the complementary strand, the base stacking of the T^{16} and T^{17} nucleobases appeared unperturbed by the presence of the N^6,N^6-dA cross-link.

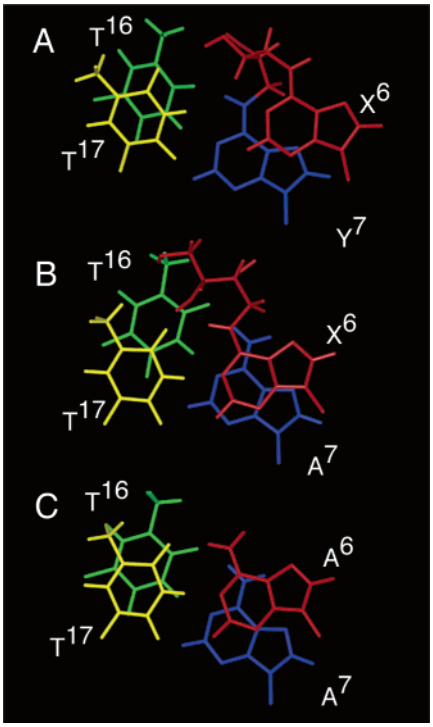

FIGURE 9: Base-stacking orientations of the (*R*,*R*)-BD-(61,2−3) cross-linked duplex. (A) The cross-linked duplex detailing base stacking of the X^6 and Y^7 base pairs. (B) The cross-linked duplex detailing base stacking of the X^6 and A^7 base pairs. (C) The unmodified *ras61* oligodeoxynucleotide duplex detailing base stacking of the A^6 and A^7 base pairs.

DISCUSSION

The genotoxicity of butadiene may be related to its ability to form cross-links in DNA via its diepoxide oxidation product. Animal studies revealed species differences between mice and rats with regard to BD genotoxicity, which mice exhibiting greater sensitivity (*7*, *8*, *87*). This was explained by the observation that in mice the conversion of BD to BDO_2 was more efficient than in rats, an observation which also pointed to BDO_2 as the key proximate electrophile in BD-mediated genotoxicity (*45*). This suspicion was confirmed by studies showing that BDO_2 was indeed considerably more mutagenic than the monoepoxide EB (*37*), probably due to its cross-linking ability. The primary evidence suggesting the presence of DBO_2-induced DNA cross-links *in vivo* comes from studies in which human lymphoblastoid TK6 and splenic T cells were exposed to low levels of BDO_2 (*37*, *88*, *89*). These experiments revealed transitions and transversions at both GC and AT sites, suggesting the presence of both dG and dA adducts arising from BDO_2. They also revealed the presence of significant levels of deletion mutants, consistent with the presence of DNA cross-links.

Structural Perturbations Associated with the N^6,N^6-dA Intrastrand Cross-Link. This intrastrand cross-link, tethering nucleotides X^6 and Y^7 in the *ras61* oligodeoxynucleotide, oriented in the major groove. That there were no interruptions in DNA sequential NOE connectivities (Figure 1), and all Watson−Crick base pairs, with the exception of base pair X^6•T^{17}, were intact (Figure 2), suggesting that the cross-link did not substantially perturb the right-handed DNA helix. Bending of the intrastrand cross-linked duplex was not

observed. This was consistent with the fact that the major groove of B-family DNA had capacity to accommodate the four-carbon cross-link. One NOE was observed between the (*R*,*R*)-N^6,N^6-dA cross-linked adduct and the DNA, an observation which was consistent with the major groove orientation of the adduct, since the major groove contains few protons as potential sources of dipolar relaxation with the BD protons. An approximate 1 ppm upfield shift of the T^{17} N3H imino proton resonance was consistent with a loss of hydrogen bonding and supported the conclusion that Watson−Crick base pairing was disrupted at base pair X^6•T^{17}. The formation of a hydrogen bond between the β-OH group of the cross-link and T^{17} O^4, predicted by the rMD calculations, possibly explained the observation of the T^{17} N3H resonance. It suggested that, in the cross-linked adduct, this non-hydrogen-bonded proton was sheltered from fast exchange with the solvent. The rMD calculations predicted that the cross-linked duplex was characterized by an increase in the β torsion angle at X^6. This facilitated opening of the duplex and enabled an approximate 5° unwinding of the duplex at base pair X^6•T^{17}. The resulting changes in stacking between cross-linked nucleotides X^6 and Y^7 possibly accounted for the upfield shift of the Y^7 H8 resonance (Figure 5).

Mechanistic Insights into Formation of N^6,N^6-dA Intrastrand Cross-Links. This N^6,N^6-dA cross-linked adduct has not yet been reported from mass spectrometry analysis of DNA exposed to BDO_2 (*49*, *54*). It is generally argued that N^6-dA alkylation products of butadiene oxides arise not by direct attack at the exocyclic amine but rather by initial alkylation at the more nucleophilic N1 imine, followed by Dimroth rearrangement to yield the N^6-dA product (*50*, *51*, *90*). One might predict that formation of an intrastrand N^6,N^6-dA cross-link would require tandem N1-dA alkylation by BDO_2 at the neighboring adenines, followed by tandem Dimroth rearrangements of both alkylated dA nucleotides. Alternatively, formation of a X^6 N1-dA adduct by BDO_2, followed by Dimroth rearrangement, would result in a N^6-dA BDO adduct (*91*, *92*). Orientation of the X^6 N^6-dA BDO adduct similar to N^6-dA butadiene triol adducts (*93*, *94*) might facilitate direct attack on the BDO epoxide by the less nucleophilic N^6-dA at the neighboring A^7. To examine this possibility, the N^6-dA BDO adduct was modeled at position X^6 on the basis of the experimentally determined solution structures of the corresponding N^6-dA BDT adducts (*93*, *94*). The modeling study (Figure 10) suggested that this might be a reasonable hypothesis. However, the initially formed N1-monoalkylated intermediate might also reorient about the glycosyl bond into the *syn* conformation. Although this has not been confirmed for the N1-dA monoalkylation product of BD, the *N*1-(1-hydroxy-3-buten-2(*S*)-yl)-2′-deoxyinosine adduct arising from deamination following N1-dA alkylation at N1-dA by BDO was accommodated in duplex DNA by rotation about the glycosyl torsion angle into the *syn* conformation (*95*, *96*). Overall, formation of the N^6,N^6-dA intrastrand cross-link seems likely to represent a rare event, with hydrolysis of the monoalkylated BDO intermediates prevailing. Indeed, the BDT N1-dA adduct was identified in humans exposed occupationally to BD (*52*). The N^6-dA BDT adduct was identified in Chinese hamster ovary cells (*53*).

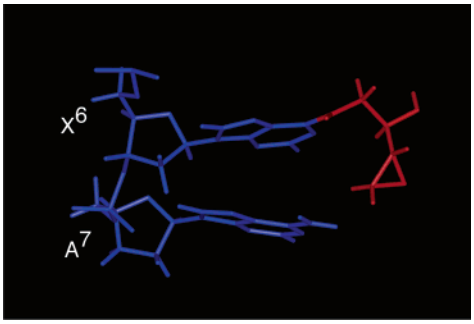

FIGURE 10: Molecular modeling of the N^6-dA BDO adduct at position X^6 of the *ras61* oligodeoxynucleotide. The X^6 BDO adduct is predicted to orient in the 3′-direction, toward the exocyclic amino group of A^7. This might faciliate direct attack by the exocyclic amine on the epoxide, leading to formation of an N^6,N^6-dA cross-link. Only nucleotides X^6 and A^7 in the modified strand of the duplex DNA are shown. The BD moiety is in red; the DNA is in blue.

Structure−Activity Relationships. The major groove orientation and the small conformational perturbation of the DNA structure induced by the cross-link are possibly correlated with facile bypass of this lesion by a variety of DNA polymerases. It was of interest to compare this cross-link structure with those of two N^6-dA butadienetriol adducts, which are products of monoalkylation at N^6-dA by BD (*93*, *94*). The monoalkylated N^6-dA BDT adducts also did not pose blocks to replication (*56*). Perhaps significantly, the *R*(61,2) and both the *R*- and *S*(61,3) N^6-dA α adducts of styrene oxide also did not pose blocks to replication (*59*, *60*) and also oriented in the major groove (*97*−*99*). The *R*- and *S*(61,2) β adducts of styrene oxide behaved similarly (*99*). Collectively, these results fit an emerging pattern in which lesion bypass by DNA polymerases is minimally affected by the presence of small major groove N^6-dA adducts, although it should be noted that the *R*(61,2) α adduct of styrene oxide did block replication (*59*). In contrast, the (*R*,*R*)- and (*S*,*S*)-N^2,N^2-dG intrastrand cross-links were severe replication blocks when examined in vitro (*61*).

The (*R*,*R*)-N^6,N^6-dA intrastrand cross-link was significantly more mutagenic than two N^6-dA BDT monoadducts previously examined as to mutagenesis (*56*) and structure (*93*, *94*). In the mammalian COS-7 site-specific mutagenesis assay the most frequent mutations were A → G transitions, followed by A → C and A → T transversions, located at the 3′-adducted dA in the tandem cross-link. In *E. coli* wild-type and AB2480 (*uvrA*-, *recA*-) cells the (*R*,*R*)-N^6,N^6-dA cross-link was significantly less mutagenic, yielding A → G transitions (*55*). Recent data suggest that, in *E. coli*, DNA polymerase II is responsible for the mutagenic bypass of the (*R*,*R*)-N^6,N^6-dA cross-link (*58*).

The observation of A → G transitions at the 3′-position of the tandem cross-link suggested that this (*R*,*R*)-N^6,N^6-dA cross-link facilitated incorrect incorporation of dCTP opposite cross-linked nucleotide Y^7. It will be of interest to examine the structure of a mismatched dC opposite the cross-link. NMR studies on mismatched dC opposite the *S*(61,2) α adduct of styrene oxide (*100*), which induced low levels of A → G mutations (*59*), and opposite the *R*- and *S*(61,3) α adducts of styrene oxide (*101*), which were nonmutagenic (*59*), revealed both sequence- and stereospecific differences in the mismatched duplexes.

The corresponding (*S*,*S*)-N^6,N^6-dA cross-link was less mutagenic in the COS-7 system (*55*, *61*). This may predict stereospecific structural differences between the (*R*,*R*)- and (*S*,*S*)-N^6,N^6-dA cross-links, and it will be of interest to compare the structure of the (*S*,*S*)-N^6,N^6-dA cross-link with that of the (*R*,*R*)-N^6,N^6-dA cross-link.

Biological Significance. When B6c3F1 *lacI* transgenic mice were exposed to butadiene, the primary adenine-specific point mutations were A → T transversions (*102*−*106*). The site-specific mutagenesis experiments on the (*R*,*R*)-N^6,N^6-dA intrastrand cross-link, yielding primarily A → G mutations (*55*), suggest that it does not represent the source of the predominant A → T BD-induced mutations in bacterial or in mammalian cells. Nonetheless, butadiene was reported to induce A → G transitions in the *H-ras* codon 61 (*107*). The (*R*,*R*)-N^6,N^6-dA cross-link may contribute to these. The *N*1-deoxyinosine adduct represents another potential source of A → G transitions. This adduct arises from deamination of the initially formed N1-dA adduct and is strongly mutagenic with respect to A → G transitions (*55*). The adducts responsible for BD-induced A → T transversions (*102*−*106*) remain to be determined. BD-induced cross-links involving monoalkylation of N7-dG (*108*−*111*) followed by cross-linking with dA (*49*) represent potential candidates.

The major BDO_2-induced DNA cross-link is the N^7,N^7-dG interstrand cross-link (*41*). It occurs in 5′-GNC-3′ sequences (*40*), as opposed to nearest-neighbor 5′-GC-3′ sequences. In this regard, BDO_2-induced N^7,N^7-dG interstrand cross-linking appears to be similar to that of the nitrogen mustard mechlorethamine (*112*). It will be of considerable interest to examine structures of N^7,N^7-dG interstrand cross-links.

Summary. The intrastrand (*R*,*R*)-N^6,N^6-dA cross-link induced by BDO_2 in duplex DNA oriented in the major groove of the duplex. It resulted in an increase in base pair opening at base pair X^6•T^{17}, accompanied by a shift in the phosphodiester backbone torsion angle β at nucleotide X^6. The DNA helix was not bent by the presence of the four-carbon cross-link. A hydrogen bond between the hydroxyl group located on the β-carbon of the four-carbon cross-link and T^{17} O^4 perhaps stabilized base pair opening at X^6•T^{17} and protected the T^{17} imino proton from solvent exchange. The opening of base pair X^6•T^{17} altered base stacking and induced unwinding of the duplex.

ACKNOWLEDGMENT

We acknowledge the contributions of Mr. Markus Voehler and Dr. Jaison Jacob, who assisted with NMR spectroscopy. Dr. Jarrod Smith assisted with structural refinement. Dr. J. R. Carmical (The University of Texas Medical Branch, Galveston) provided helpful discussions.

SUPPORTING INFORMATION AVAILABLE

Table S1, showing the ^{1}H chemical shift assignments for the *ras61* (*R*,*R*)-N^6,N^6-dA cross-link, Table S2, showing the NOE restraints utilized in the rMD calculations for the (*R*,*R*)-N^6,N^6-dA cross-link, and Figure S1, showing force field parameters for the (*R*,*R*)-N^6,N^6-dA cross-link. This material is available free of charge via the Internet at http://pubs.acs.org.

REFERENCES

1. Himmelstein, M. W., Acquavella, J. F., Recio, L., Medinsky, M. A., and Bond, J. A. (1997) Toxicology and epidemiology of 1,3-butadiene, *Crit. Rev. Toxicol. 27*, 1−108.
2. Jackson, M. A., Stack, H. F., Rice, J. M., and Waters, M. D. (2000) A review of the genetic and related effects of 1,3-butadiene in rodents and humans, *Mutat. Res. 463*, 181−213.
3. Pelz, N., Dempster, N. M., and Shore, P. R. (1990) Analysis of low molecular weight hydrocarbons including 1,3-butadiene in engine exhaust gases using an aluminum oxide porous-layer open-tubular fused-silica column, *J. Chromatogr. Sci. 28*, 230−235.
4. Brunnemann, K. D., Kagan, M. R., Cox, J. E., and Hoffmann, D. (1990) Analysis of 1,3-butadiene and other selected gas-phase components in cigarette mainstream and sidestream smoke by gas chromatography−mass selective detection, *Carcinogenesis 11*, 1863−1868.
5. Huff, J. E., Melnick, R. L., Solleveld, H. A., Haseman, J. K., Powers, M., and Miller, R. A. (1985) Multiple organ carcinogenicity of 1,3-butadiene in B6c3F1 mice after 60 weeks of inhalation exposure, *Science 227*, 548−549.
6. Melnick, R. L., Huff, J., Chou, B. J., and Miller, R. A. (1990) Carcinogenicity of 1,3-butadiene in C57BL/6 x C3H F1 mice at low exposure concentrations, *Cancer Res. 50*, 6592−6599.
7. Melnick, R. L., Huff, J. E., Roycroft, J. H., Chou, B. J., and Miller, R. A. (1990) Inhalation toxicology and carcinogenicity of 1,3-butadiene in B6c3F1 mice following 65 weeks of exposure, *Environ. Health Perspect. 86*, 27−36.
8. Owen, P. E., and Glaister, J. R. (1990) Inhalation toxicity and carcinogenicity of 1,3-butadiene in Sprague-Dawley rats, *Environ. Health Perspect. 86*, 19−25.
9. United States Environmental Protection Agency (2002) 1,3-Butadiene. Carcinogenicity assessment for lifetime exposure: Weight-of-evidence characterization (http://www.epa.gov/iris/subst/0139.htm).
10. International Agency for Research on Cancer (1999) Re-evaluation of some organic chemicals, hydrazine and hydrogen peroxide, IRC Monographs on the Evaluation of Carcinogenic Risks to Humans, *IARC Sci. Publ. 71*, 109−125.
11. Bird, M. G., Rice, J. M., and Bond, J. A. (2001) Evaluation of 1,3-butadiene, isoprene and chloroprene health risks, *Chem.-Biol. Interact. 135*−*136*, 1−7.
12. Rice, J. M., and Boffetta, P. (2001) 1,3-Butadiene, isoprene and chloroprene: Reviews by the IARC monographs programme, outstanding issues, and research priorities in epidemiology, *Chem.-Biol. Interact. 135*−*136*, 11−26.
13. Ward, J. B., Jr., Ammenheuser, M. M., Bechtold, W. E., Whorton, E. B., Jr., and Legator, M. S. (1994) *Hprt* mutant lymphocyte frequencies in workers at a 1,3-butadiene production plant, *Environ. Health Perspect. 102* (Suppl.) *9*, 79−85.
14. Ward, J. B., Jr., Ammenheuser, M. M., Whorton, E. B., Jr., Bechtold, W. E., Kelsey, K. T., and Legator, M. S. (1996) Biological monitoring for mutagenic effects of occupational exposure to butadiene, *Toxicology 113*, 84−90.
15. Sram, R. J., Rossner, P., Peltonen, K., Podrazilova, K., Mrackova, G., Demopoulos, N. A., Stephanou, G., Vlachodimitropoulos, D., Darroudi, F., and Tates, A. D. (1998) Chromosomal aberrations, sister-chromatid exchanges, cells with high frequency of SCE, micronuclei and comet assay parameters in 1,3-butadiene-exposed workers, *Mutat. Res. 419*, 145−154.
16. Delzell, E., Sathiakumar, N., Hovinga, M., Macaluso, M., Julian, J., Larson, R., Cole, P., and Muir, D. C. (1996) A follow-up study of synthetic rubber workers, *Toxicology 113*, 182−189.
17. Meinhardt, T. J., Lemen, R. A., Crandall, M. S., and Young, R. J. (1982) Environmental epidemiologic investigation of the styrene-butadiene rubber industry. Mortality patterns with discussion of the hematopoietic and lymphatic malignancies, *Scand. J. Work Environ. Health 8*, 250−259.
18. Matanoski, G., Francis, M., Correa-Villasenor, A., Elliott, E., Santos-Burgoa, C., and Schwartz, L. (1993) Cancer epidemiology among styrene-butadiene rubber workers, *IARC Sci. Publ. 127*, 363−374.
19. Santos-Burgoa, C., Matanoski, G. M., Zeger, S., and Schwartz, L. (1992) Lymphohematopoietic cancer in styrene-butadiene polymerization workers, *Am. J. Epidemiol. 136*, 843−854.
20. Macaluso, M., Larson, R., Delzell, E., Sathiakumar, N., Hovinga, M., Julian, J., Muir, D., and Cole, P. (1996) Leukemia and

cumulative exposure to butadiene, styrene and benzene among workers in the synthetic rubber industry, *Toxicology 113*, 190−202.
21. Matanoski, G. M., and Schwarts, L. (1987) Mortality of workers in styrene-butadiene polymer production, *J. Occup. Med. 29*, 675−680.
22. Santos-Burgoa, C., Eden-Wynter, R. A., Riojas-Rodriguez, H., and Matanoski, G. M. (1997) Living in a chemical world. Health impact of 1,3-butadiene carcinogenesis, *Ann. N.Y. Acad. Sci. 837*, 176−188.
23. Matanoski, G., Elliott, E., Tao, X., Francis, M., Correa-Villasenor, A., and Santos-Burgoa, C. (1997) Lymphohematopoietic cancers and butadiene and styrene exposure in synthetic rubber manufacture, *Ann. N.Y. Acad. Sci. 837*, 157−169.
24. Albertini, R., Clewell, H., Himmelstein, M. W., Morinello, E., Olin, S., Preston, J., Scarano, L., Smith, M. T., Swenberg, J., Tice, R., and Travis, C. (2003) The use of non-tumor data in cancer risk assessment: Reflections on butadiene, vinyl chloride, and benzene, *Regul. Toxicol. Pharmacol. 37*, 105−132.
25. Csanady, G. A., Guengerich, F. P., and Bond, J. A. (1992) Comparison of the biotransformation of 1,3-butadiene and its metabolite, butadiene monoepoxide, by hepatic and pulmonary tissues from humans, rats and mice, *Carcinogenesis 13*, 1143−1153 [erratum: (1993) *Carcinogenesis 14*, 784].
26. Duescher, R. J., and Elfarra, A. A. (1994) Human liver microsomes are efficient catalysts of 1,3-butadiene oxidation: Evidence for major roles by cytochromes P450 2A6 and 2E1, *Arch. Biochem. Biophys. 311*, 342−349.
27. Malvoisin, E., Evrard, E., Roberfroid, M., and Mercier, M. (1979) Determination of Kovats retention indices with a capillary column and electron-capture detection: Application to the assay of the enzymatic conversion of 3,4-epoxy-1-butene into diepoxybutane, *J. Chromatogr. 186*, 81−87.
28. Seaton, M. J., Follansbee, M. H., and Bond, J. A. (1995) Oxidation of 1,2-epoxy-3-butene to 1,2:3,4-diepoxybutane by cDNA-expressed human cytochromes P450 2E1 and 3A4 and human, mouse and rat liver microsomes, *Carcinogenesis 16*, 2287−2293.
29. Malvoisin, E., and Roberfroid, M. (1982) Hepatic microsomal metabolism of 1,3-butadiene, *Xenobiotica 12*, 137−144.
30. Himmelstein, M. W., Turner, M. J., Asgharian, B., and Bond, J. A. (1994) Comparison of blood concentrations of 1,3-butadiene and butadiene epoxides in mice and rats exposed to 1,3-butadiene by inhalation, *Carcinogenesis 15*, 1479−1486.
31. Himmelstein, M. W., Asgharian, B., and Bond, J. A. (1995) High concentrations of butadiene epoxides in livers and lungs of mice compared to rats exposed to 1,3-butadiene, *Toxicol. Appl. Pharmacol. 132*, 281−288.
32. Cheng, X., and Ruth, J. A. (1993) A simplified methodology for quantitation of butadiene metabolites. Application to the study of 1,3-butadiene metabolism by rat liver microsomes, *Drug. Metab. Dispos. 21*, 121−124.
33. Nauhaus, S. K., Fennell, T. R., Asgharian, B., Bond, J. A., and Sumner, S. C. (1996) Characterization of urinary metabolites from Sprague-Dawley rats and B6c3F1 mice exposed to [1,2,3,4-^{13}C]-butadiene, *Chem. Res. Toxicol. 9*, 764−773.
34. Kemper, R. A., Elfarra, A. A., and Myers, S. R. (1998) Metabolism of 3-butene-1,2-diol in B6c3F1 mice. Evidence for involvement of alcohol dehydrogenase and cytochrome P450, *Drug Metab. Dispos. 26*, 914−920.
35. Boogaard, P. J., and Bond, J. A. (1996) The role of hydrolysis in the detoxification of 1,2:3,4-diepoxybutane by human, rat, and mouse liver and lung *in vitro*, *Toxicol. Appl. Pharmacol. 141*, 617−627.
36. Powley, M. W., Jayaraj, K., Gold, A., Ball, L. M., and Swenberg, J. A. (2003) 1,N^2-propanodeoxyguanosine adducts of the 1,3-butadiene metabolite, hydroxymethylvinyl ketone, *Chem. Res. Toxicol. 16*, 1448−1454.
37. Cochrane, J. E., and Skopek, T. R. (1994) Mutagenicity of butadiene and its epoxide metabolites: I. Mutagenic potential of 1,2-epoxybutene, 1,2,3,4-diepoxybutane and 3,4-epoxy-1,2-butanediol in cultured human lymphoblasts, *Carcinogenesis 15*, 713−717.
38. Brookes, P., and Lawley, P. D. (1961) The reaction of mono and di-functional alkylating agents with nucleic acids, *Biochem. J. 80*, 496−503.
39. Lawley, P. D., and Brookes, P. (1967) Interstrand cross-linking of DNA by difunctional alkylating agents, *J. Mol. Biol. 25*, 143−160.
40. Millard, J. T., and White, M. M. (1993) Diepoxybutane cross-links DNA at 5′-GNC sequences, *Biochemistry 32*, 2120−2124.
41. Park, S., and Tretyakova, N. (2004) Structural characterization of the major DNA-DNA cross-link of 1,2,3,4-diepoxybutane, *Chem. Res. Toxicol. 17*, 129−136.
42. Vangala, R. R., Laib, R. J., and Bolt, H. M. (1993) Evaluation of DNA damage by alkaline elution technique after inhalation exposure of rats and mice to 1,3-butadiene, *Arch. Toxicol. 67*, 34−38.
43. Ristau, C., Deutschmann, S., Laib, R. J., and Ottenwalder, H. (1990) Detection of diepoxybutane-induced DNA-DNA crosslinks by cesium trifluoracetate (CsTFA) density-gradient centrifugation, *Arch. Toxicol. 64*, 343−344.
44. Thornton-Manning, J. R., Dahl, A. R., Bechtold, W. E., Griffith, W. C. J., and Henderson, R. F. (1997) Comparison of the disposition of butadiene epoxides in Sprague-Dawley rats and B6c3F1 mice following a single and repeated exposures to 1,3-butadiene via inhalation, *Toxicology 123*, 125−134.
45. Thornton-Manning, J. R., Dahl, A. R., Bechtold, W. E., Griffith, W. C., Jr., and Henderson, R. F. (1995) Disposition of butadiene monoepoxide and butadiene diepoxide in various tissues of rats and mice following a low-level inhalation exposure to 1,3-butadiene, *Carcinogenesis 16*, 1723−1731.
46. Wickliffe, J. K., Ammenheuser, M. M., Salazar, J. J., Abdel-Rahman, S. Z., Hastings-Smith, D. A., Postlethwait, E. M., Lloyd, R. S., and Ward, J. B., Jr. (2003) A model of sensitivity: 1,3-butadiene increases mutant frequencies and genomic damage in mice lacking a functional microsomal epoxide hydrolase gene, *Environ. Mol. Mutagen. 42*, 106−110.
47. Abdel-Rahman, S. Z., Ammenheuser, M. M., and Ward, J. B., Jr. (2001) Human sensitivity to 1,3-butadiene: Role of microsomal epoxide hydrolase polymorphisms, *Carcinogenesis 22*, 415−423.
48. Abdel-Rahman, S. Z., El-Zein, R. A., Ammenheuser, M. M., Yang, Z., Stock, T. H., Morandi, M., and Ward, J. B., Jr. (2003) Variability in human sensitivity to 1,3-butadiene: Influence of the allelic variants of the microsomal epoxide hydrolase gene, *Environ. Mol. Mutagen. 41*, 140−146.
49. Park, S., Hodge, J., Anderson, C., and Tretyakova, N. (2004) Guanine-adenine DNA cross-linking by 1,2,3,4-diepoxybutane: Potential basis for biological activity, *Chem. Res. Toxicol. 17*, 1638−1651.
50. Qian, C., and Dipple, A. (1995) Different mechanisms of aralkylation of adenosine at the 1- and N^6-positions, *Chem. Res. Toxicol. 8*, 389−395.
51. Kim, H. Y., Finneman, J. I., Harris, C. M., and Harris, T. M. (2000) Studies of the mechanisms of adduction of 2′-deoxyadenosine with styrene oxide and polycyclic aromatic hydrocarbon dihydrodiol epoxides, *Chem. Res. Toxicol. 13*, 625−637.
52. Zhao, C., Vodicka, P., Sram, R. J., and Hemminki, K. (2000) Human DNA adducts of 1,3-butadiene, an important environmental carcinogen. *Carcinogenesis 21*, 107−111.
53. Leuratti, C., Jones, N. J., Marafante, E., Kostiainen, R., Peltonen, K., and Waters, R. (1994) DNA damage induced by the environmental carcinogen butadiene: identification of a diepoxybutane-adenine adduct and its detection by ^{32}P-postlabelling, *Carcinogenesis 15*, 1903−1910.
54. Tretyakova, N., Sangaiah, R., Yen, T. Y., Gold, A., and Swenberg, J. A. (1997) Adenine adducts with diepoxybutane: Isolation and analysis in exposed calf thymus DNA, *Chem. Res. Toxicol. 10*, 1171−1179.
55. Kanuri, M., Nechev, L. V., Tamura, P. J., Harris, C. M., Harris, T. M., and Lloyd, R. S. (2002) Mutagenic spectrum of butadiene-derived N1-deoxyinosine adducts and N^6,N^6-deoxyadenosine intrastrand cross-links in mammalian cells, *Chem. Res. Toxicol. 15*, 1572−1580.
56. Carmical, J. R., Nechev, L. V., Harris, C. M., Harris, T. M., and Lloyd, R. S. (2000) Mutagenic potential of adenine N^6 adducts of monoepoxide and diolepoxide derivatives of butadiene, *Environ. Mol. Mutagen. 35*, 48−56.
57. Carmical, J. R., Zhang, M., Nechev, L., Harris, C. M., Harris, T. M., and Lloyd, R. S. (2000) Mutagenic potential of guanine N^2 adducts of butadiene mono- and diolepoxide, *Chem. Res. Toxicol. 13*, 18−25 [erratum: (2000) *Chem. Res. Toxicol. 13*, 430].
58. Kanuri, M., Nechev, L. V., Kiehna, S. E., Tamura, P. J., Harris, C. M., Harris, T. M., and Lloyd, R. S. (2005) Evidence for *Escherichia coli* polymerase II mutagenic bypass of intrastrand DNA crosslinks, *DNA Repair* (in press).
59. Latham, G. J., Zhou, L., Harris, C. M., Harris, T. M., and Lloyd, R. S. (1993) The replication fate of *R*- and *S*-styrene oxide adducts

on adenine N^6 is dependent on both the chirality of the lesion and the local sequence context, *J. Biol. Chem. 268*, 23427−23434.
60. Kanuri, M., Harris, C. M., Harris, T. M., and Lloyd, R. S. (2001) Efficient non-mutagenic replication bypass of DNAs containing β-styrene oxide N^6-adenine adducts, *Environ. Mol. Mutagen. 38*, 357−360.
61. Carmical, J. R., Kowalczyk, A., Zou, Y., Van Houten, B., Nechev, L. V., Harris, C. M., Harris, T. M., and Lloyd, R. S. (2000) Butadiene-induced intrastrand DNA cross-links: A possible role in deletion mutagenesis, *J. Biol. Chem. 275*, 19482−19489.
62. Nechev, L. V., Zhang, M., Tsarouhtsis, D., Tamura, P. J., Wilkinson, A. S., Harris, C. M., and Harris, T. M. (2001) Synthesis and characterization of nucleosides and oligonucleotides bearing adducts of butadiene epoxides on adenine N^6 and guanine N^2, *Chem. Res. Toxicol. 14*, 379−388.
63. Borer, P. N. (1975) in *Handbook of Biochemistry and Molecular Biology*, CRC Press, Cleveland, OH.
64. Piotto, M., Saudek, V., and Sklenar, V. (1992) Gradient-tailored excitation for single-quantum NMR spectroscopy of aqueous solutions, *J. Biomol. NMR 2*, 661−665.
65. Bax, A., and Davis, D. G. (1985) MLEV-17-based two-dimensional homonuclear magnetization transfer spectroscopy, *J. Magn. Reson. 65*, 355−360.
66. James, T. L. (1991) Relaxation matrix analysis of two-dimensional nuclear Overhauser effect spectra, *Curr. Opin. Struct. Biol. 1*, 1042−1053.
67. Keepers, J. W., and James, T. L. (1984) A theoretical study of distance determination from NMR. Two-dimensional nuclear Overhauser effect spectra, *J. Magn. Reson. 57*, 404−426.
68. Borgias, B. A., and James, T. L. (1989) Two-dimensional nuclear Overhauser effect: Complete relaxation matrix analysis, *Methods Enzymol. 176*, 169−183.
69. Borgias, B. A., and James, T. L. (1990) MARDIGRAS—a procedure for matrix analysis of relaxation for discerning geometry of an aqueous structure, *J. Magn. Reson. 87*, 475−487.
70. Liu, H., Spielmann, H. P., Ulyanov, N. B., Wemmer, D. E., and James, T. L. (1995) Interproton distance bounds from 2D NOE intensities: effect of experimental noise and peak integration errors, *J. Biomol. NMR 6*, 390−402.
71. Wang, H., Zuiderweg, E. R. P., and Glick, G. D. (1995) Solution structure of a disulfide cross-linked DNA hairpin, *J. Am. Chem. Soc. 117*, 2981−2991.
72. Geen, H., and Freeman, R. (1991) Band-selective radiofrequency pulses, *J. Magn. Reson. 93*, 93−141.
73. Lankhorst, P. P., Haasnoot, A. G., Erkelens, C., and Altona, C. (1984) Carbon-13 NMR in conformational analysis of nucleic acid fragments. 3. The magnitude of torsional angle in d(TpA) from CCOP and HCOP NMR coupling constants, *Nucleic Acids Res. 12*, 5419−5428.
74. Arnott, S., and Hukins, D. W. L. (1972) Optimised parameters for A-DNA and B-DNA, *Biochem. Biophys. Res. Commun. 47*, 1504−1509.
75. Case, D. A., Pearlman, D. A., Caldwell, J. W., Cheatham, T. E., III, Wang, J., Ross, W. S., Simmerling, C. L., Darden, T. A., Merz, K. M., Stanton, R. V., Cheng, A. L., Vincent, JJ., Crowley, M., Tsui, V., Gohlke, H., Radmer, R. J., Duan, Y., Pitera, J., Massova, I., Seibel, G. L., Singh, U. C., Weiner, P. K., Kollman, P. A. (2002) AMBER 7.0, University of California, San Francisco, CA.
76. Clore, G. M., Brunger, A. T., Karplus, M., and Gronenborn, A. M. (1986) Application of molecular dynamics with interproton distance restraints to three-dimensional protein structure determination, *J. Mol. Biol. 191*, 523−551.
77. Ryckaert, J.-P., Ciccotti, G., and Berendsen, H. J. C. (1977) Numerical integration of the Cartesian equations of motion of a system with constraints: Molecular dynamics of *n*-alkanes, *J. Comput. Phys. 23*, 327−341.
78. Bashford, D., and Case, D. A. (2000) Generalized Born models of macromolecular solvation effects, *Annu. Rev. Phys. Chem. 51*, 129−152.
79. Tsui, V., and Case, D. A. (2000) Theory and applications of the generalized Born solvation model in macromolecular simulations, *Biopolymers 56*, 275−291.
80. Cornell, W. D., Cieplak, P., Bayly, C. I., Gould, I. R., Merz, K. M., Ferguson, D. M., Spellmeyer, D. C., Fox, T., Caldwell, J. W., and Kollman, P. A. (1995) A second generation force field for the simulation of proteins, nucleic acids, and organic molecules, *J. Am. Chem. Soc. 117*, 5179.
81. Lu, X. J., and Olson, W. K. (2003) 3DNA: A software package for the analysis, rebuilding and visualization of three-dimensional nucleic acid structures, *Nucleic Acids Res. 31*, 5108−5121.
82. Patel, D. J., Shapiro, L., and Hare, D. (1987) DNA and RNA: NMR studies of conformations and dynamics in solution, *Q. Rev. Biophys. 20*, 35−112.
83. Reid, B. R. (1987) Sequence-specific assignments and their use in NMR studies of DNA structure, *Q. Rev. Biophys. 20*, 2−28.
84. Feng, B., and Stone, M. P. (1995) Solution structure of an oligodeoxynucleotide containing the human N-ras codon 61 sequence refined from ^{1}H NMR using molecular dynamics restrained by nuclear overhauser effects, *Chem. Res. Toxicol. 8*, 821−832.
85. Nikonowicz, E. P., and Gorenstein, D. G. (1990) Two-dimensional ^{1}H and ^{31}P NMR spectra and restrained molecular dynamics structure of a mismatched GA decamer oligodeoxyribonucleotide duplex, *Biochemistry 29*, 8845−8858.
86. Koo, H. S., and Crothers, D. M. (1988) Calibration of DNA curvature and a unified description of sequence-directed bending, *Proc. Natl. Acad. Sci. U.S.A. 85*, 1763−1767.
87. Jelitto, B., Vangala, R. R., and Laib, R. J. (1989) Species differences in DNA damage by butadiene: Role of diepoxybutane, *Arch. Toxicol., Suppl. 13*, 246−249.
88. Cochrane, J. E., and Skopek, T. R. (1993) Mutagenicity of 1,3-butadiene and its epoxide metabolites in human TK6 cells and in splenic T cells isolated from exposed B6c3F1 mice, *IARC Sci. Publ. 127*, 195−204.
89. Cochrane, J. E., and Skopek, T. R. (1994) Mutagenicity of butadiene and its epoxide metabolites: II. Mutational spectra of butadiene, 1,2-epoxybutene and diepoxybutane at the hprt locus in splenic T cells from exposed B6c3F1 mice, *Carcinogenesis 15*, 719−723.
90. Selzer, R. R., and Elfarra, A. A. (1996) Characterization of N1- and N^6-adenosine adducts and N1-inosine adducts formed by the reaction of butadiene monoxide with adenosine: Evidence for the N1-adenosine adducts as major initial products, *Chem. Res. Toxicol. 9*, 875−881.
91. Tretyakova, N., Lin, Y., Sangaiah, R., Upton, P. B., and Swenberg, J. A. (1997) Identification and quantitation of DNA adducts from calf thymus DNA exposed to 3,4-epoxy-1-butene, *Carcinogenesis 18*, 137−147.
92. Tretyakova, N., Lin, Y. P., Upton, P. B., Sangaiah, R., and Swenberg, J. A. (1996) Macromolecular adducts of butadiene, *Toxicology 113*, 70−76.
93. Scholdberg, T. A., Nechev, L. V., Merritt, W. K., Harris, T. M., Harris, C. M., Lloyd, R. S., and Stone, M. P. (2004) Structure of a site specific major groove (2*S*,3*S*)-N^6-(2,3,4-trihydroxybutyl)-2′-deoxyadenosyl DNA adduct of butadiene diol epoxide, *Chem. Res. Toxicol. 17*, 717−730.
94. Merritt, W. K., Scholdberg, T. A., Nechev, L. V., Harris, T. M., Harris, C. M., Lloyd, R. S., and Stone, M. P. (2004) Stereospecific structural perturbations arising from adenine N^6 butadiene triol adducts in duplex DNA, *Chem. Res. Toxicol. 17*, 1007−1019.
95. Scholdberg, T. A., Merritt, W. K., Dean, S. M., Kowalcyzk, A., Harris, C. M., Harris, T. M., Lloyd, R. S., Stone, M. P. (2005) Structure of an oligodeoxynucleotide containing a butadiene oxide-derived N1 β-hydroxyalkyl deoxyinosine adduct in the human *N-ras* codon 61 sequence, *Biochemistry 44*, 3327−3337.
96. Merritt, W. K., Kowalczyk, A., Scholdberg, T. A., Dean, S. M., Harris, T. M., Harris, C. M., Lloyd, R. S., and Stone, M. P. (2005) Dual roles of stereochemical configuration and glycosyl torsion angle conformation upon trans-lesion replication of butadiene oxide-derived N1 β-hydroxyalkyl deoxyinosine adducts: A structural perspective, *Chem. Res. Toxicol.* (in press).
97. Feng, B., Voehler, M. W., Zhou, L., Passarelli, M., Harris, C. M., Harris, T. M., and Stone, M. P. (1996) Major groove *S*-α-(N^6-adenyl)-styrene oxide adducts in an oligodeoxynucleotide containing the human N-ras codon 61 sequence: Conformations of the *S*(61,2) and *S*(61,3) sequence isomers from ^{1}H NMR, *Biochemistry 35*, 7316−7329.
98. Feng, B., Zhou, L., Passarelli, M., Harris, C. M., Harris, T. M., and Stone, M. P. (1995) Major groove (*R*)-α-(N^6-adenyl)styrene oxide adducts in an oligodeoxynucleotide containing the human N-ras codon 61 sequence: Conformations of the *R*(61,2) and *R*(61,3) sequence isomers from ^{1}H NMR, *Biochemistry 34*, 14021−14036.
99. Hennard, C., Finneman, J., Harris, C. M., Harris, T. M., and Stone, M. P. (2001) The nonmutagenic (*R*)- and (*S*)-β-(N^6-adenyl)styrene

oxide adducts are oriented in the major groove and show little perturbation to DNA structure, *Biochemistry 40*, 9780−9791.
100. Painter, S. L., Zegar, I. S., Tamura, P. J., Bluhm, S., Harris, C. M., Harris, T. M., and Stone, M. P. (1999) Influence of the *R*(61,2)- and *S*(61,2)-α-(N^6-adenyl)styrene oxide adducts on the A:C mismatched base pair in an oligodeoxynucleotide containing the human N-ras codon 61, *Biochemistry 38*, 8635−8646.
101. Simeonov, M. F., Tamura, P. J., Wilkinson, A. S., Harris, C. M., Harris, T. M., and Stone, M. P. (2000) Sequence- and stereospecific conformational rearrangement of styrene oxide adducts located at A x C mismatched base pairs, *Biochemistry 39*, 924−937.
102. Recio, L., Saranko, C. J., and Steen, A. M. (2000) 1,3-Butadiene: Cancer, mutations, and adducts. Part II: Roles of two metabolites of 1,3-butadiene in mediating its in vivo genotoxicity, *Res. Rep.—Health Eff. Inst.*, 49−87, 141−149 (discussion).
103. Recio, L., Steen, A. M., Pluta, L. J., Meyer, K. G., and Saranko, C. J. (2001) Mutational spectrum of 1,3-butadiene and metabolites 1,2-epoxybutene and 1,2,3,4-diepoxybutane to assess mutagenic mechanisms, *Chem.-Biol. Interact. 135*−*136*, 325−341.
104. Sisk, S. C., Pluta, L. J., Bond, J. A., and Recio, L. (1994) Molecular analysis of *lacI* mutants from bone marrow of B6c3F1 transgenic mice following inhalation exposure to 1,3-butadiene, *Carcinogenesis 15*, 471−477.
105. Recio, L., and Meyer, K. G. (1995) Increased frequency of mutations at A:T base pairs in the bone marrow of B6c3F1 *lacI* transgenic mice exposed to 1,3-butadiene, *Environ. Mol. Mutagen. 26*, 1−8.
106. Steen, A. M., Meyer, K. G., and Recio, L. (1997) Analysis of *hprt* mutations occurring in human TK6 lymphoblastoid cells following exposure to 1,2,3,4-diepoxybutane, *Mutagenesis 12*, 61−67.
107. Goodrow, T. L., Nichols, W. W., Storer, R. D., Anderson, M. W., and Maronpot, R. R. (1994) Activation of H-ras is prevalent in 1,3-butadiene-induced and spontaneously occurring murine Harderian gland tumors, *Carcinogenesis 15*, 2665−2667.
108. Tretyakova, N. Yu., Chiang, S. Y., Walker, V. E., and Swenberg, J. A. (1998) Quantitative analysis of 1,3-butadiene-induced DNA adducts *in vivo* and *in vitro* using liquid chromatography electrospray ionization tandem mass spectrometry, *J. Mass Spectrom. 33*, 363−376.
109. Tretyakova, N. Yu., Lin, Y. P., Upton, P. B., Sangaiah, R., and Swenberg, J. A. (1996) Macromolecular adducts of butadiene, *Toxicology 113*, 70−76.
110. Tretyakova, N. Yu., Sangaiah, R., Yen, T. Y., and Swenberg, J. A. (1997) Synthesis, characterization, and in vitro quantitation of N-7-guanine adducts of diepoxybutane, *Chem. Res. Toxicol. 10*, 779−785.
111. Selzer, R. R., and Elfarra, A. A. (1999) *In vitro* reactions of butadiene monoxide with single- and double-stranded DNA: Characterization and quantitation of several purine and pyrimidine adducts, *Carcinogenesis 20*, 285−292.
112. Millard, J. T., Raucher, S., and Hopkins, P. B. (1990) Mechlorethamine cross-links deoxyguanosine residues at 5′-GNC sequences in duplex DNA fragments, *J. Am. Chem. Soc. 112*, 2459−2460.

BI047263G